# 1 Lagrangian Tracking of the Central Arctic Regional Sea Ice Transport to the North-East Atlantic basins

## 1.1 Methodology

### 1.1.1 Overview of sea ice thickness change tracking methodology

In this study, the Lagrangian tracking of ice thickness change is implemented using the CESM1.2 Los Alamos Sea Ice Model, version 5 (CICE5) [*Hunke and Lipscomb*, 2015]. This implementation is useful in tracking the trajectories of the growth and melt cycle of regional Arctic sea ice. CICE5 uses the mechanical redistribution scheme of *Lipscomb et al.* [2007]. It also includes elastic-viscous-plastic rheology [*Hunke and Dukowicz*, 1997, 2002] and subgrid ice thickness distribution, with a default of five thickness categories. CICE5 uses default mushy-layer thermodynamics [*Turner and Hunke*, 2015; *Bailey et al.*, 2020] in which the sea ice is treated as a mushy layer that includes microscopic brine surrounded by a matrix of pure-water ice. Additionally, mushy-layer thermodynamics solves the bulk sea ice salinity profile as a prognostic variable [*Turner and Hunke*, 2015]. In general, sea ice grows by both thermodynamic and mechanical processes [*Hibler*, 1988]; however, this study focuses on tracking the dynamic change of sea ice grown only due to the thermodynamic process. Therefore, the proposed implementation uses thermodynamic components from the CICE5.

An important characteristic of sea ice thermodynamics is the variation in growth and melting rates for different ice thickness ranges. Thermodynamic growth and melting balance the energy at the top surface and beneath the ice cover, along with internal heat conduction and storage. Ice growth or melting at the bottom surface results from the difference between heat conducted away from the boundary into the ice and the heat flux supplied from the ocean. Therefore, the thermodynamic components contributing to sea ice growth are condensation, congelation growth (or basal ice), frazil ice formation, and snow ice formation, while the thermodynamic components contributing to the sea ice loss are surface melt, bottom melt, lateral melt, and sublimation.

The growth processes increase sea ice volume by altering the effects on ice thickness and area. Unlike the growth processes, the melt processes contribute to open water formation, by reducing ice volume and have direct implications on ice thickness and area. These growth and melt processes affect the exchanges of mass (fresh water) and energy with the atmosphere and ocean. Melt processes are efficient at open water formation where thin ice is dominant, and they are useful to identify regions for studying ice-albedo feedback [*Smith et al.*, 2021].

Since the sea-ice mass balance encompasses local growth, local melt, horizontal transport, and deformation, this study proposes 18 passive (i.e., independent) tracers in the CICE5 corresponding to 18 sub-Arctic basins (source regions; Fig. 1.1) to track the regional sea ice growth and corresponding advected (or melted) ice. In other words, these tracers decompose the ice thickness into ice growth (inside source region) and melt (outside source region). This formulation is useful in tracking the regions of ice thickness change only stemming from growth (source) or melt (outside) independently. The net growth is computed by subtracting the total ice growth (source) from the total melt (outside). First, to initiate the Lagrangian tracking of sea ice thickness change resulting only from the ice growth, total thermodynamic growth is tagged for each of the 18 source regions (Fig. 1.1), as shown in Equation 1.3. Then, the melt (Eqn. 1.5) condition is applied to initiate sea ice advection resulting from the effect of changes in ice dynamics (i.e., divergence and deformation). Initially, the tracking begins from zero, which means that the tracer begins to accumulate thickness change from zero. The sea ice thickness change ($P_{ice}$) formulation is computed using the total thermodynamic growth rates ($dh_{TG}$) and melt rates ($dh_{TM}$):

$$dh_{TG}=dh_{congel-bottom} + dh_{snoice-top} + dh_{cond} + dh_{frazil-lateral} \tag{1.1}$$

where the first, second, third, and fourth terms on the right-hand side of the equation describe the thickness change due to the bottom, top, condensation, and lateral growth, respectively.

And,

$$dh_{TM}=dh_{melt-bottom}+dh_{melt-top}+dh_{sublim}+dh_{melt-lateral} \tag{1.2}$$

where the first, second, third, and fourth terms on the right-hand side of the equation describe the thickness change due to the bottom, top, sublimation, and lateral melt, respectively.

**Step 1**:

$$PG_{ice}^{t+1}(i,j,k)=PG_{ice}^{t}(i,j,k)+dh_{TG}(i,j), \tag{1.3}$$

where k =1, 2, 3....., 18. where k indicates that the tracking of growth is initiated independently for each source region (see, Fig. 1.1). $PG_{ice}$ represents the ice thickness change only due to the thermodynamic growth.

$$P_{ice}(i,j,k)=PG_{ice}(i,j,k), \tag{1.4}$$

**Step 2**:

$$P_{ice}^{t+1}(i,j,:)=\begin{cases} P_{ice}^{t}(i,j,:)-\zeta(i,j)*P_{ice}^{t}(i,j,:), & if \quad \zeta(i,j)\leqslant 1 \; and \quad dh_{gd}(i,j)>0, \\ 0, & Otherwise \end{cases} \tag{1.5}$$

where $\zeta(i,j)=\frac{dh_{TM}(i,j)}{dh_{gd}(i,j)}$,

and $dh_{gd}(i,j)$ = $h_{final}(i,j)$ - $h_{initial}(i,j)$,

$dh_{gd}(i,j)$ represents the total change in grid cell thickness. $h_{final}(i,j)$ stands for maximum ice thickness at each grid cell while $h_{initial}(i,j)$ stands for initial ice thickness at each

grid cell.

Overall, $P_{ice}$ tracks the total ice thickness change at each grid cell. Eqns. 1.3 and 1.5 are formulated to initiate the tracking of sea ice growth, melt, and advected ice of each source region independently. The melting of sea ice is applied proportionately, such that nether the melt ($dh_{TM}$) nor the total thickness ($P_{ice}(i,j,k)$) does not exceed the total change in grid cell thickness ($dh_{gd}(i,j)$). This ensures that the amount of ice entering the grid cell is equivalent to the amount of ice that leaves the grid cell in all source regions. This is to avoid the inhibition of the numerical simulation due to the conservation error. The sea ice volume ($km^3$) can be derived by multiplying the thickness value associated with each source region by its areal ice coverage. The tracers can be interpreted either using the Eulerian representation, where the sea ice is treated as a spatially fixed volume element, or the Lagrangian representation, where the motion of the fluid element changes over time.

In thickness space, grid cells move forward in time when a vertical change in ice thickness occurs. At the same time, sea ice exchange occurs between grid cells due to horizontal transport. In CICE5, the horizontal transport of sea ice is accomplished using the incremental remapping scheme [*Lipscomb and Hunke*, 2004]. During horizontal transport, if ice motion is dominated by either divergent or convergent forces, then the ice might be transported or retained in the grid cells, respectively. Similar to other sea ice tracers in CICE5 [*Hunke and Lipscomb*, 2015], the conservation of sea ice thickness change under horizontal transport is described as follows:

$$\frac{\partial(P_{ice})}{\partial t} + \nabla \cdot (P_{ice}\mathbf{u}) = 0 \tag{1.6}$$

### 1.1.2 Model description and experiment

This study uses the Community Earth System Model (CESM) 1.2 to simulate a set of decadal simulations. The CESM-LENS experiment as described in *Kay et al.* [2015a] is used to produce 10-member future scenario simulations. These 10-member simulations are integrated from 2011 to 2020. The CESM future scenario simulation is based on CESM, version 1.2, using the same model and component configuration used in the CESM-LENS [*Kay et al.*, 2015b; *Yeager et al.*, 2018]. The fully coupled CESM1.2 model integrates atmosphere component from the Community Atmosphere Model, version 5 (CAM5; *Hurrell et al.* [2013]), the ocean component from the Parallel Ocean Program, version 2 (POP2; *Danabasoglu et al.* [2012]), the land component from the Community Land Model, version 4 (CLM4; *Lawrence* [2011], and the sea ice component from the Los Alamos National Laboratory (LANL) Community Ice Code, version 5, (CICE5; *Hunke and Lipscomb* [2015]).

The atmosphere component has a one-degree horizontal resolution with a finite-volume dynamical core and 30 vertical levels. The ocean component has a one-degree horizontal resolution and 60 vertical levels. The future scenario projections (from 2011 onward) use radiative forcings that are identical to those used in CESM-LE [*Kay et al.*, 2015b; *Yeager et al.*, 2018]. However, in this study, the external forcing is set to constant. Initial conditions for the atmosphere, run off, ocean, ice and land models were obtained from each of the 10 members (001,002,003.....010) of the CESM-LE projection run, from which the January 1, 2011 restart files were saved. For each restart, a 10-member ensemble was generated by randomly perturbing the atmospheric initial condition at the round-off level. The simulations were integrated forward for 120 months after initialization. The CESM-LE runs are forced by CMIP5 RCP8.5 radiative forcing (or a scenario of comparatively high greenhouse gas emissions). Note that the internal variability that arises from small differences in initial conditions influences each ensemble member more than the atmospheric initial conditions do. Analyses of the sea ice thickness change of each basin are presented using the 10-member future scenario simulations.

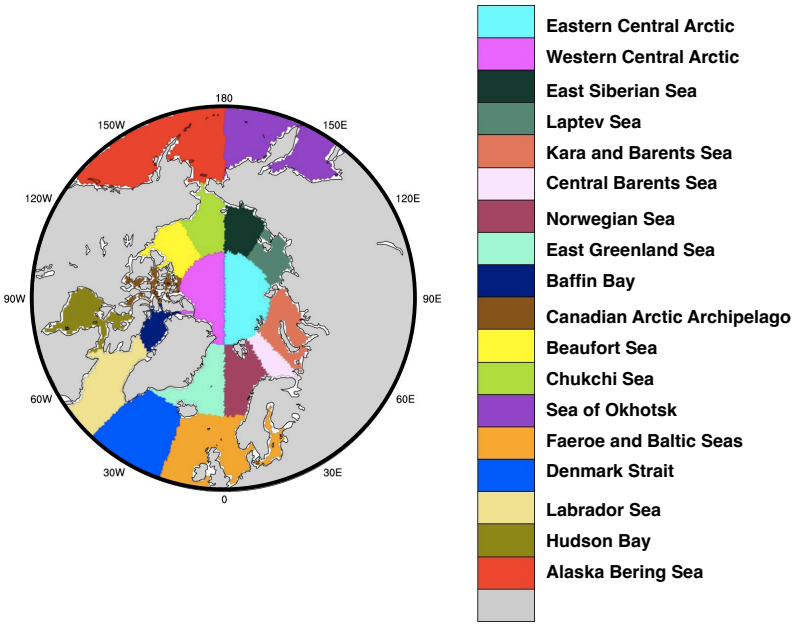


Figure 1.1: Map of the 18 different polygon regions (source) where the tracking of sea ice is initiated.

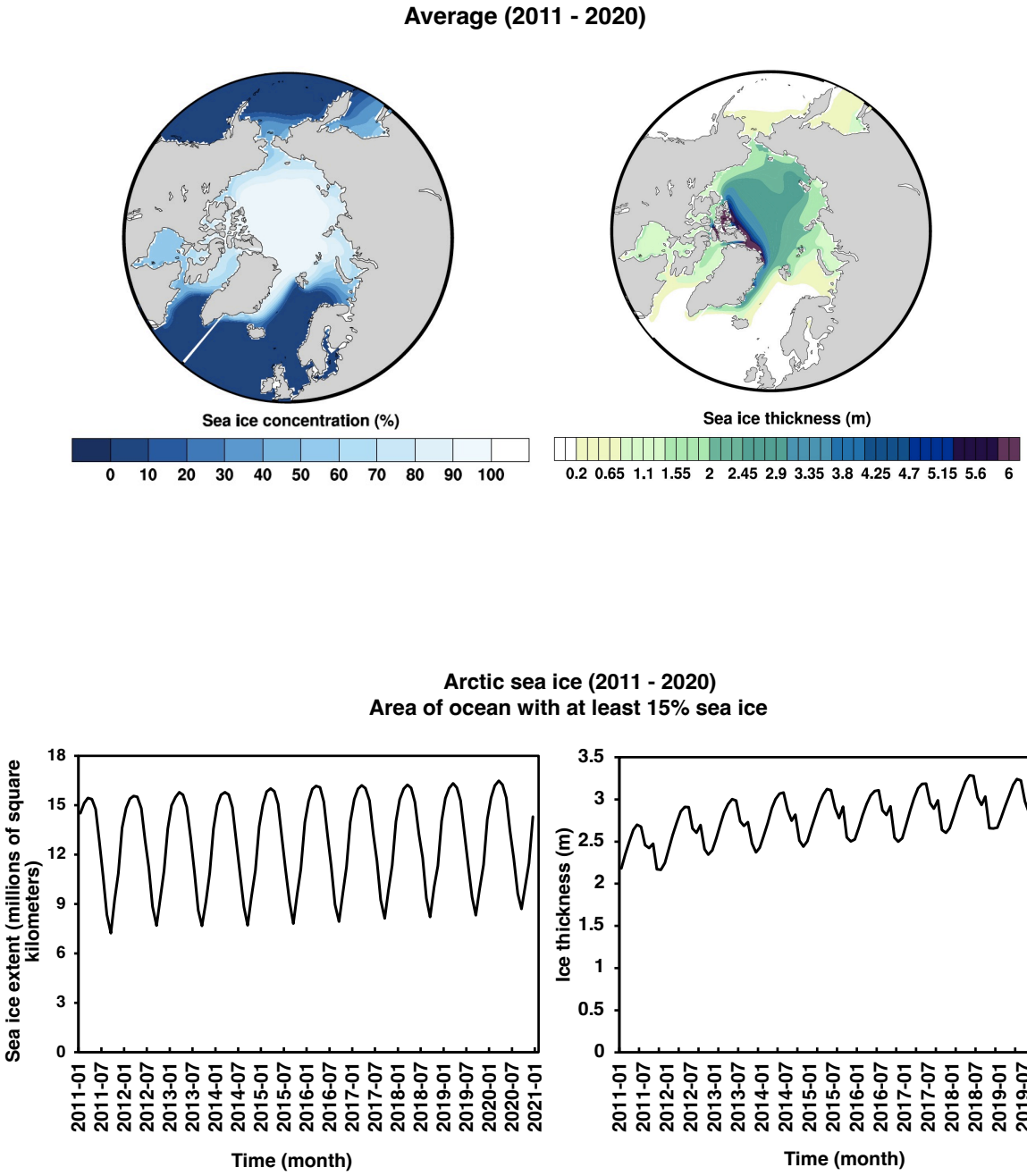


Figure 1.2: Spatial map of ensemble average (2011-2020) of (top left) the sea ice concentration (%) and (top right) sea ice thickness (m). Time series of total (bottom left) sea ice extent (millions of square kilometers) and (bottom right) sea ice thickness (m) for the Arctic Ocean with at least 15% sea ice. Future scenario 10-member simulations with constant external forcing are analyzed.

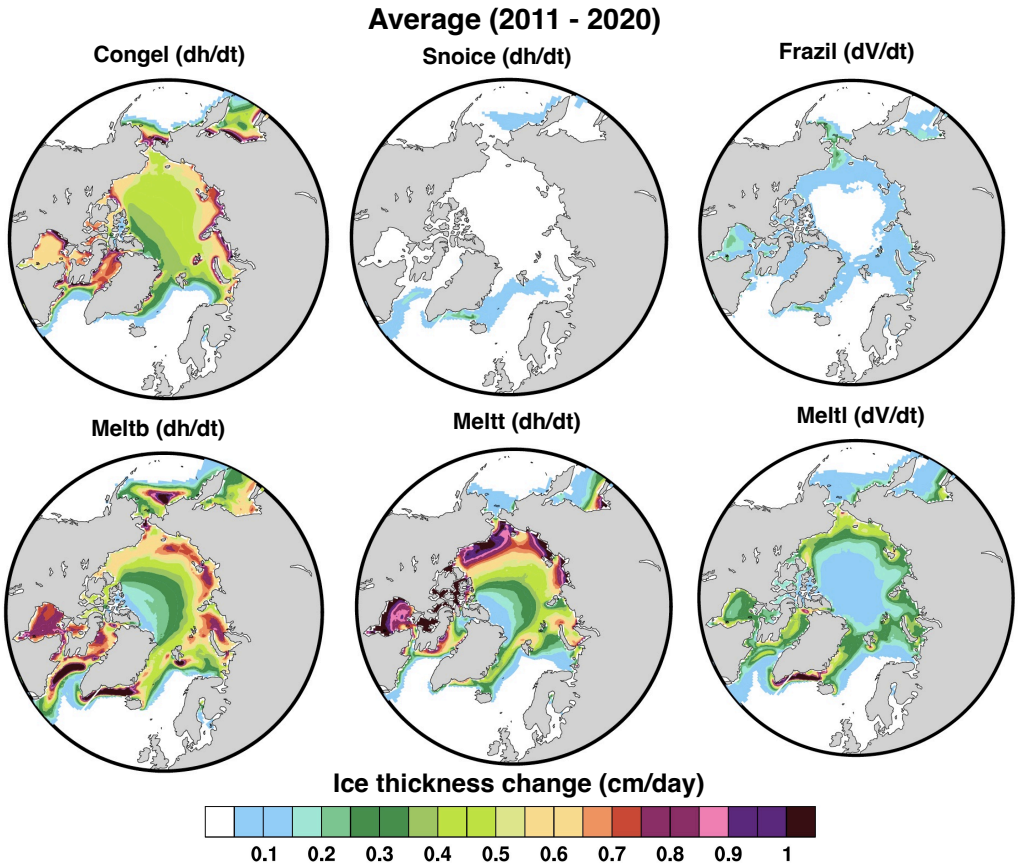


Figure 1.3: (top left) Spatial map of ensemble average (2011-2020) of ice thickness change because of (top left) congelation growth (cm/day), (top middle) snow ice growth (cm/day), (top right) frazil ice growth (cm/day), (bottom left) bottom melt (cm/day), (bottom middle) top melt (cm/day), and (bottom right) lateral melt (cm/day).

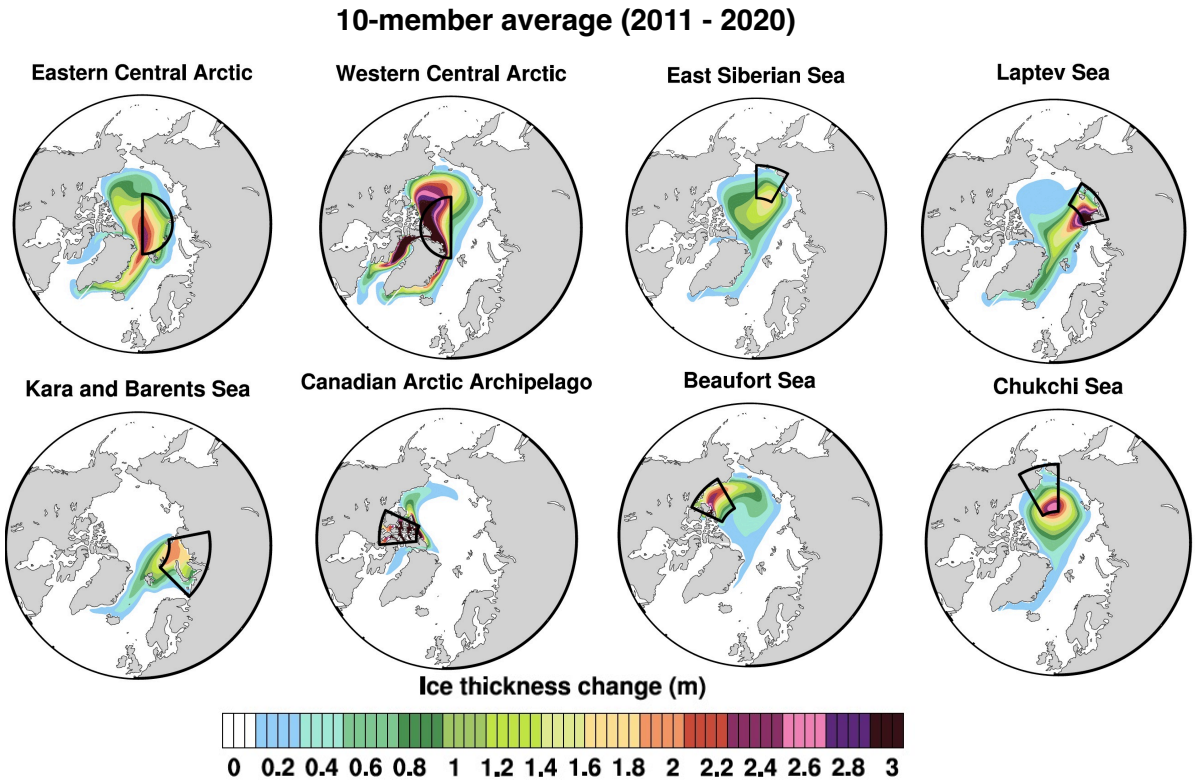


Figure 1.4: Spatial map of ensemble average (2011-2020) of sea ice thickness change inside (growth only) and outside (melt only) the source regions. The source regions are highlighted with black polygons to distinguish them from the corresponding melt ice regions.

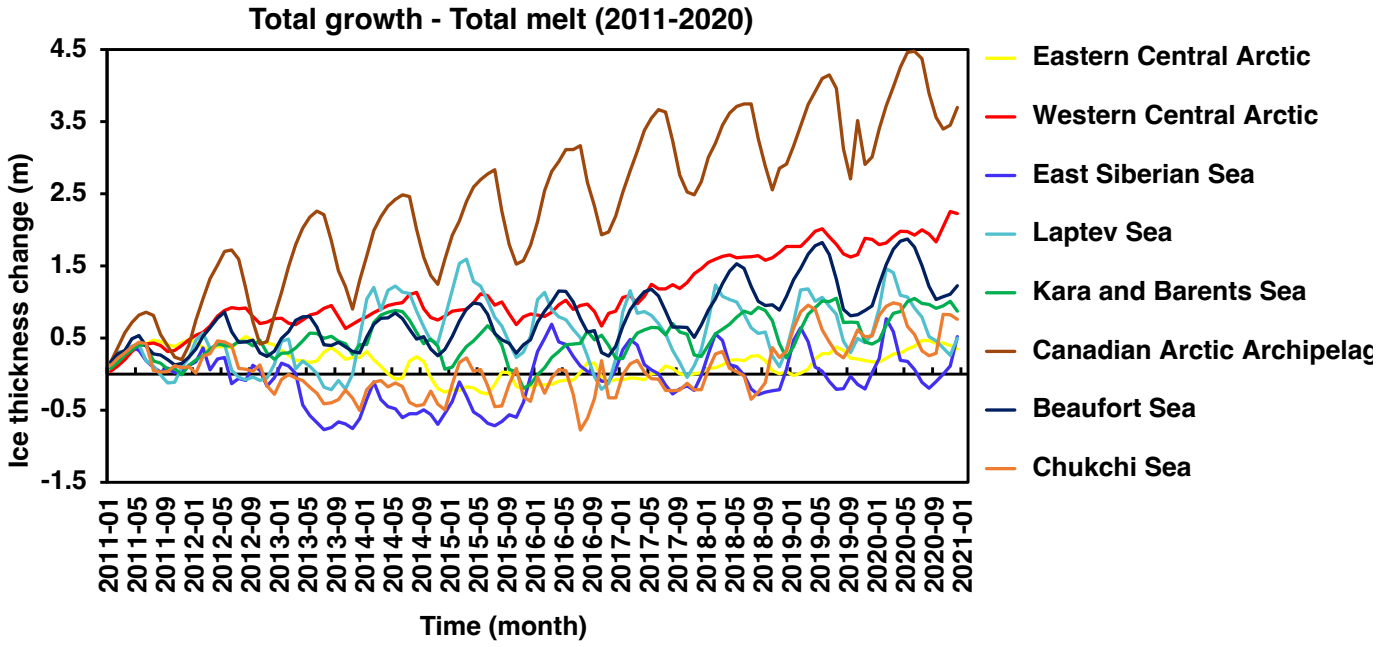


Figure 1.5: Time series of ensemble average (2011-2020) of sea ice thickness change because of the net growth for each of the central Arctic basins.

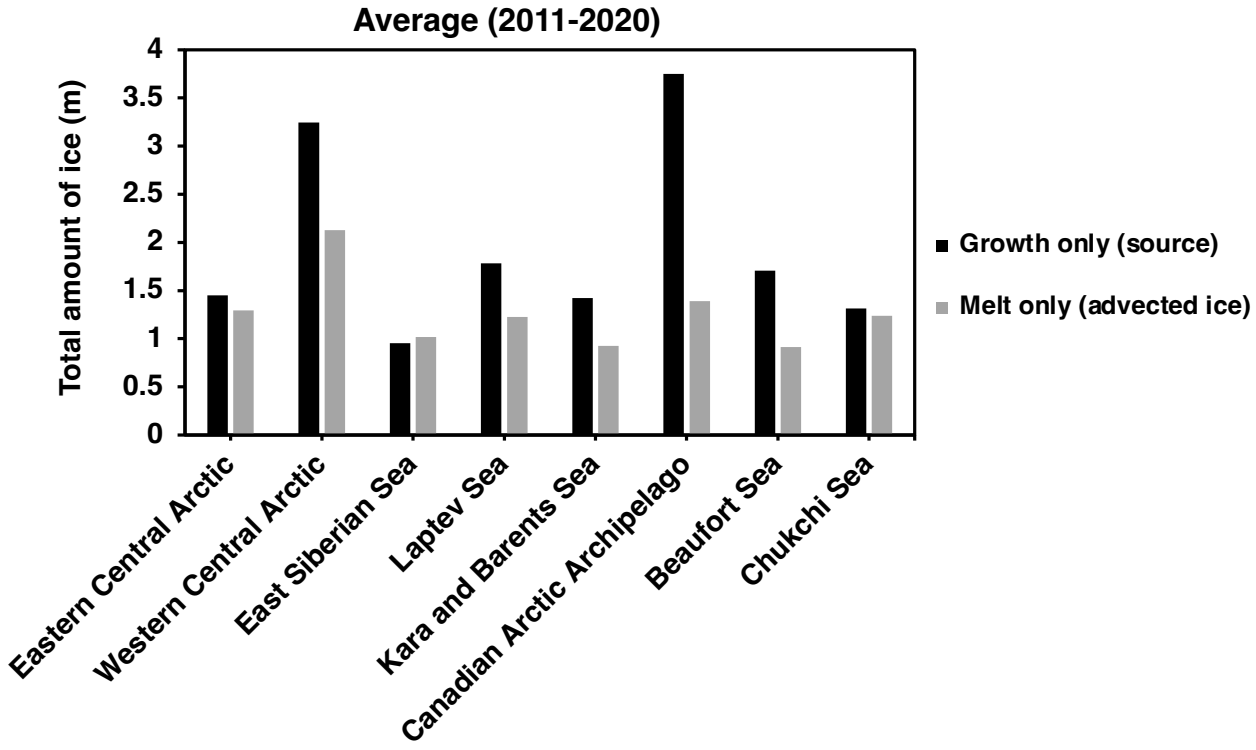


Figure 1.6: Time series of ensemble average (2011-2020) of total amount of ice inside (growth only) and outside (melt only) the source regions.

References

Bailey, D. A., M. M. Holland, A. K. DuVivier, E. C. Hunke, and A. K. Turner (2020), Impact of a new sea ice thermodynamic formulation in the cesm2 sea ice component, *Journal of Advances in Modeling Earth Systems*, *12*(11), e2020MS002,154, doi:https://doi.org/10.1029/2020MS002154.

Danabasoglu, G., S. C. Bates, B. P. Briegleb, S. R. Jayne, M. Jochum, W. G. Large, S. Peacock, and S. G. Yeager (2012), The ccsm4 ocean component, *Journal of Climate*, *25*(5), 1361 – 1389, doi:10.1175/JCLI-D-11-00091.1.

Hibler, W. D. (1988), Modelling sea ice thermodynamics and dynamics in climate studies, in *Physically-Based Modelling and Simulation of Climate and Climatic Change: Part 1*, edited by M. E. Schlesinger, NATO ASI Series, pp. 509–563, Dordrecht, doi:10.1007/978-94-009-3041-4_12.

Hunke, E. C., and J. K. Dukowicz (1997), An elastic–viscous–plastic model for sea ice dynamics, *Journal of Physical Oceanography*, *27*(9), 1849–1867.

Hunke, E. C., and J. K. Dukowicz (2002), The Elastic–Viscous–Plastic Sea Ice Dynamics Model in General Orthogonal Curvilinear Coordinates on a Sphere—Incorporation of Metric Terms, *Monthly Weather Review*, *130*(7), 1848–1865, doi:10.1175/1520-0493(2002)130⟨1848:TEVPSI⟩2.0.CO;2, publisher: American Meteorological Society Section: Monthly Weather Review.

Hunke, E. C., and W. H. Lipscomb (2015), CICE: the Los Alamos sea ice model documentation and software user's manual version 4.0, p. 73.

Hurrell, J. W., M. M. Holland, P. R. Gent, S. Ghan, J. E. Kay, P. J. Kushner, J.-F. Lamarque, W. G. Large, D. Lawrence, K. Lindsay, W. H. Lipscomb, M. C. Long, N. Mahowald, D. R. Marsh, R. B. Neale, P. Rasch, S. Vavrus, M. Vertenstein, D. Bader, W. D. Collins,

J. J. Hack, J. Kiehl, and S. Marshall (2013), The Community Earth System Model: A framework for collaborative research, *Bulletin of the American Meteorological Society*, *94*(9), 1339–1360, doi:10.1175/BAMS-D-12-00121.1, publisher: American Meteorological Society Section: Bulletin of the American Meteorological Society.

Kay, J. E., C. Deser, A. Phillips, A. Mai, C. Hannay, G. Strand, J. M. Arblaster, S. C. Bates, G. Danabasoglu, and J. Edwards (2015a), The Community Earth System Model (CESM) large ensemble project: A community resource for studying climate change in the presence of internal climate variability, *Bulletin of the American Meteorological Society*, *96*(8), 1333–1349.

Kay, J. E., C. Deser, A. Phillips, A. Mai, C. Hannay, G. Strand, J. M. Arblaster, S. C. Bates, G. Danabasoglu, J. Edwards, M. Holland, P. Kushner, J.-F. Lamarque, D. Lawrence, K. Lindsay, A. Middleton, E. Munoz, R. Neale, K. Oleson, L. Polvani, and M. Vertenstein (2015b), The Community Earth System Model (CESM) Large Ensemble Project: A community resource for studying climate change in the presence of internal climate variability, *Bulletin of the American Meteorological Society*, *96*(8), doi:10.1175/BAMS-D-13-00255.1.

Lawrence, D. M. (2011), Parameterization improvements and functional and structural advances in version 4 of the community land model, *J. Adv. Model. Earth Syst.*, *3*, M03,001.

Lipscomb, W. H., and E. C. Hunke (2004), Modeling sea ice transport using incremental remapping, *Monthly Weather Review*, *132*(6), doi:10.1175/1520-0493(2004)132⟨1341:MSITUI⟩2.0.CO;2.

Lipscomb, W. H., E. C. Hunke, W. Maslowski, and J. Jakacki (2007), Ridging, strength, and stability in high-resolution sea ice models, *Journal of Geophysical Research: Oceans*, *112*(C3), doi:https://doi.org/10.1029/2005JC003355.

Smith, M., M. Holland, and B. Light (2021), Arctic sea ice sensitivity to lateral melting representation in acoupled climate model, *preprint*, Sea ice/Sea Ice, doi:10.5194/tc-2021-67.

Turner, A. K., and E. C. Hunke (2015), Impacts of a mushy-layer thermodynamic approach in global sea-ice simulations using the cice sea-ice model, *Journal of Geophysical Research: Oceans*, *120*(2), 1253–1275, doi:https://doi.org/10.1002/2014JC010358.

Yeager, S. G., G. Danabasoglu, N. A. Rosenbloom, W. Strand, S. C. Bates, G. A. Meehl, A. R. Karspeck, K. Lindsay, M. C. Long, H. Teng, and N. S. Lovenduski (2018), Predicting near-term changes in the earth system: A large ensemble of initialized decadal prediction simulations using the community earth system model, *Bulletin of the American Meteorological Society*, *99*(9), 1867 – 1886, doi:10.1175/BAMS-D-17-0098.1.